Precipitate formation in low-temperature nitrided cold-rolled Fe94Ni4Ti2 and Fe93Ni4Cr3 films

Chechenin, N.G.; Chezan, A.R; Craus, C.B.; Boerma, D.O; Bronsveld, P.M; de Hosson, J.T.M.; Niesen, L

Published in:
Metallurgical and Materials Transactions A-Physical Metallurgy and Materials Science

DOI:
10.1007/s11661-002-0292-1

Publication date:
2002

Precipitate Formation in Low-Temperature Nitrided Cold-Rolled $Fe_{94}Ni_4Ti_2$ and $Fe_{93}Ni_4Cr_3$ Films

N.G. CHECHENIN, A.R. CHEZAN, C.B. CRAUS, D.O. BOERMA, P.M. BRONSVELD, J.Th.M.DE HOSSON, and L. NIESEN

Using various experimental techniques, the formation and evolution of precipitates, the dilation of the matrix, and the nitrogen uptake and release were investigated in cold-rolled $Fe_{94}Ni_4Ti_2$ and $Fe_{93}Ni_4Cr_3$ materials subjected to nitriding in a gaseous mixture of $NH_3 + H_2$ and to reduction in an H_2 atmosphere at low (300 °C) to moderate (600 °C) temperatures. Transmission electron microscopy (TEM) revealed that in both alloys the precipitates are thin platelets. In the Ti-containing alloy, the precipitates were also small in the lateral dimensions. The difference in size, aspect ratio of the precipitates, and misfit and coherency on the interface consistently explain the substantial differences in dilation of the matrix and nitrogen uptake for the Ti- and Cr-containing alloys under examination. The results provide evidence for the formation of mixed Fe-Ti-N precipitates (Guinier–Preston (GP) zones) in the early stages of nitriding.

I. INTRODUCTION

SINCE the early 1930s, the effect of nitrides in a metal matrix on the hardness, durability, and other useful properties of iron alloys has been an important field of interest. It was realized that an increase in hardness was due to a very fine dispersion of nitrides of alloying elements that distorted the crystal lattice of iron so much as to lead to slip interference,[1] that is, to the interaction of dislocations with coherency strain fields around precipitates. The microstructure of iron alloys before and after nitriding has been studied intensively in the past decades, specifically with the advances in transmission electron microscopy (TEM). It has been concluded from early TEM and X-ray diffraction (XRD) studies that, because of a large affinity to nitrogen, some of the alloying elements, such as Cr,[2,3] Ti,[4–8] V,[9,10] or Mo,[11,12] easily form thin and stable precipitates on the {100} faces of the bcc Fe lattice and, thus, influence the mechanical properties of the alloy. The reported thickness of the precipitates varies from one monolayer to tens of nanometers. However, the initial stage of precipitate formation is still under debate. In publications of the Newcastle researchers,[11,13–16] a substitutional-interstitial pre-precipitation phase Fe-M-N is assumed to occur in a nitrided Fe-M alloy before a stable MN phase precipitates, where M = Cr, Ti, V, or Mo and are alloying elements in a concentration below ~5 at. pct. Such embryonic precipitates are local inhomogeneities, called mixed clusters or Guinier–Preston (GP) zones. There are doubts, however, if such zones have really been observed[4,17] and whether the idea of such clusters is necessary to explain the experimental observations.

N.G. CHECHENIN, Leading Scientist, Skobeltsyn Institute of Nuclear Physics, Moscow State University, 119899 Moscow, Russia, is Visiting Professor, Nuclear Solid State Physics Group, Materials Science Centre, University of Groningen, NL 9747 AG Groningen, The Netherlands. Contact e-mail: chechenin@phys.rug.nl A.R. CHEZAN and C.B. CRAUS, Postdoctoral Students, and D.O. BOERMA and L. NIESEN, Professors, Nuclear Solid State Physics Group, Materials Science Centre, and P.M. BRONSVELD, Associate Professor, and J.Th.M.De HOSSON, Professor, Applied Physics Department, Materials Science Centre, are with the University of Groningen.

Manuscript submitted September 10, 2001.

Another uncertainty in the process of precipitate formation is whether, or under what conditions, the precipitates are located at the grain boundaries or in the bulk. A discontinuous (at the grain boundaries) precipitation of CrN has been observed[18] in thick FeCr (1.9 and 3.6 wt pct Cr) samples, nitrided in the α region at 560 °C. Also, the growth of CrN precipitates at grain boundaries has been reported for alloys containing more than 5 wt pct Cr, nitrided at 600 °C.[3] Precipitation at grain boundaries has the negative effect of reducing the hardness and increasing brittleness of the nitrided samples. Cold working prior to nitriding was shown to prevent the formation of precipitates at the grain boundaries and to enhance the mechanical properties for a nitrided Fe-Ti (0.18 wt pct) alloy.[7]

The fcc-precipitates CrN and TiN are found to follow the Bain orientation relationship (OR) with the bcc matrix, namely, (100)bcc//(100)fcc and [001]bcc//[01$\bar{1}$]fcc. The misfits at the interface plane (100), $\varepsilon_{//} = (a_{MN}/\sqrt{2} - a_{\alpha Fe})/a_{\alpha Fe} = 0.046$ (TiN) and 0.0204 (CrN), are small, but in the perpendicular direction, the misfits, $\varepsilon_{\perp,\,1/1} = (a_{MN} - a_{\alpha Fe} = 0.48$ (TiN) and 0.45 (CrN), are large. Two units of αFe lattice match, with one fcc unit somewhat better, and three units of αFe match well with two fcc units, as shown in Table I. Nevertheless, the average fit to metal atoms is poor in the perpendicular direction. The large difference between parallel and perpendicular misfits promotes platelike shapes of the (semi)coherent precipitates.

Our approach to the subject of precipitate formation differs from the previous ones in several aspects, namely, in sample preparation (thin foils, 99 pct reduction in thickness by cold rolling without annealing before nitriding), in nitriding (lower temperatures and precise control of the nitriding conditions), and in the combination of analyzing techniques, which include microbalance weighing, Mössbauer spectroscopy (MS), XRD, and TEM. Based on these observations, the present results provide additional clues about precipitate formation in steels. In this article, a model of formation and evolution of precipitates is presented that explains contrasting observations on matrix dilations and nitrogen uptake for the nitrided Ti- and Cr-containing alloys. The results provide supporting evidence for the formation of GP-like

Table I. Misfits and Orientation Relationship between fcc Precipitates and bcc Matrix

Interface	a_{MN}, nm	$\varepsilon_{//}$*	$\varepsilon_{\perp,1/1}$**	$\varepsilon_{\perp,1/2}$†	$\varepsilon_{\perp,2/3}$‡	OR
TiN/αFe	0.424	0.046	0.48	−0.26	−0.015	(100)bcc//(100)fcc, [001]bcc//[01$\bar{1}$]fcc
CrN/αFe	0.414	0.0204	0.45	−0.28	−0.039	(100)bcc//(100)fcc, [001]bcc//[011]fcc

*$\varepsilon_{//} = (a_{MN}/\sqrt{2} - a_{\alpha Fe})/a_{\alpha Fe}$
**$\varepsilon_{\perp,1/1} = (a_{MN} - a_{\alpha Fe})/a_{\alpha Fe}$
†$\varepsilon_{\perp,1/2} = (a_{MN} - 2a_{\alpha Fe})/2a_{\alpha Fe}$
‡$\varepsilon_{\perp,2/3} = (2a_{MN} - 3a_{\alpha Fe})/3a_{\alpha Fe}$

clusters of Fe-Ti-N in an early stage of nitriding. There is, however, no evidence for the formation of GP zones in Fe-Cr-N. Throughout, the influence of the Ni present in our samples has not been considered. Because the Ni is atomically dissolved and has an interaction with N that is even weaker than the interaction between N and Fe, we believe that the influence of Ni on the precipitation processes is minor.

II. EXPERIMENTAL

A. *Specimen Preparation*

Slices (0.5-mm thick) of bulk $Fe_{94}Ni_4Ti_2$ and $Fe_{93}Ni_4Cr_3$ alloys were polished and chemically cleaned prior to cold rolling in two perpendicular directions down to a foil thickness of 1 to 6 μm. A high-temperature annealing was not applied, neither before or after rolling. Therefore, a severe pileup of defects, induced by such a strong plastic deformation, was assumed to be in the samples prior to the nitriding. Subsequently, foils were nitrided during a period between 1 and 24 hours at a temperature in the range 300 °C to 600 °C in a clean, closed oven, described in Reference 19, with a gaseous mixture of $NH_3 + H_2$ of 1 atm circulating by convection. Normally, nitriding at low temperatures near 300 °C is hampered by the presence of trace amounts of oxygen or water in the system, causing oxidation rather than nitriding. By continuously leading the gas over sodium metal, this problem is not present in the system we used. The partial gas pressures and the temperature were controlled with an accuracy of 1 mb and 1 °C, respectively. The process is called α nitriding (αN) because the temperature, T, and nitriding potential, $R_N = \ln [p(NH_3)/p(H_2)^{3/2}]$, where the pressures of ammonia, $p(NH_3)$, and hydrogen, $p(H_2)$, are in Pascals, correspond to the α region of the Fe-N Lehrer phase diagram,[19,20,21] where no formation of stoichiometric Fe nitrides is expected. After nitriding, some of the samples were reduced in a hydrogen atmosphere at $T = 300$ °C to 700 °C.

B. *Characterization Techniques*

The nitrogen content in the foils was determined by weighing, using a Mettler Instrumenten MT5 electronic balance with a precision of 1 μg. The phase composition and texture in the samples were characterized by XRD, using a PHILIPS* PW1710 spectrometer for ϑ-2ϑ scans.

*PHILIPS is a trademark of Philips Analytical, Almelo, The Netherlands.

Mössbauer spectrometry was used to characterize the local environment of Fe atoms in the lattice by studying the magnetic hyperfine field. Conventional TEM was performed with a JEOL* 200CX microscope using an accelerating voltage of 200 kV. High-resolution TEM (HRTEM) was carried out with a JEOL 4000EX/II electron microscope with an accelerating voltage of 400 kV. Before inspection in TEM, the samples were thinned by two-beam Ar^+-ion milling until perforation. After milling, the samples were exposed to air for a period of less than 5 minutes. Nevertheless, in some cases, oxidation of the surface was observed in TEM diffraction patterns (DPs). The results of positron annihilation, carried out on selected samples, are in a good correspondence with the present results and have been published elsewhere.[22]

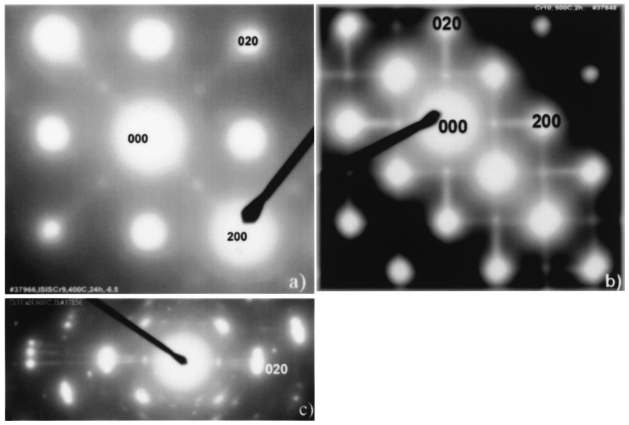

Fig. 1—Streaking in DP for Fe_{93} Ni_4 Cr_3. Nitriding was in the α region of the Lehrer diagram: (*a*) 400 °C, 24 h, and $R_N = -6.5$; (*b*) 500 °C, 2 h, and $R_N = -7.3$; (*c*) 600 °C, 1 h, and $R_N = -8.1$, in a multicrystallite area. Streaking was not observed after nitriding at 300 °C.

*JEOL is a trademark of Japan Electron Optics Ltd., Tokyo.

III. RESULTS

A. *Characterization of the Shape and Size of Precipitates*

Nitriding of $Fe_{93}Ni_4Cr_3$ and $Fe_{94}Ni_4Ti_2$ samples in the region below the γ'/α or γ/α borders in the Lehrer diagram leads to the formation of M*N* precipitates, leaving the matrix in the bcc or in the bct structure, as has already been discussed in Section I. The platelets, coherently grown on {100} cube faces of the α-Fe lattice, with a thickness of one to several monolayers, appear as {200} streaks in the TEM DP (Figures 1 through 3) in accordance with the Bain OR. The length of the streaks is inversely proportional to the thickness of the precipitate (Appendix) so when the thickness is more than a few lattice parameters, the length of the streaks

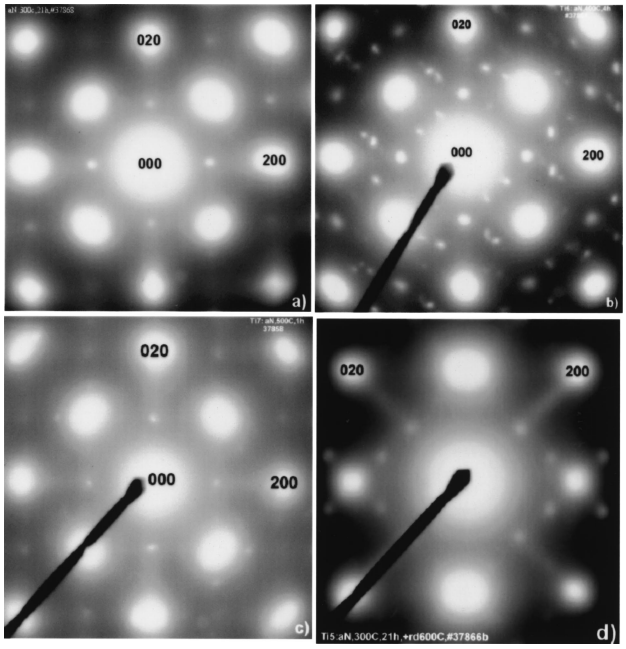

Fig. 2—Streaking in DP for $Fe_{94}Ni_4Ti_2$. Nitriding conditions were as follows: (*a*) 300 °C, 21 h, and $R_N = -5.08$; (*b*) 400 °C, 20 h, and $R_N = -6.78$, (*c*) 500 °C, 1 h, and $R_N = -7.3$; (*d*) 300 °C, 21 h, and $R_N = -5.08$, and then reduced at 600 °C, 16 h, in H2 atmosphere. Compared with the Cr-containing alloy, streaking in the Ti-containing alloy starts at a lower nitriding temperature and time, but is weaker and more diffuse. Reduction at 600 °C makes the streaking sharper.

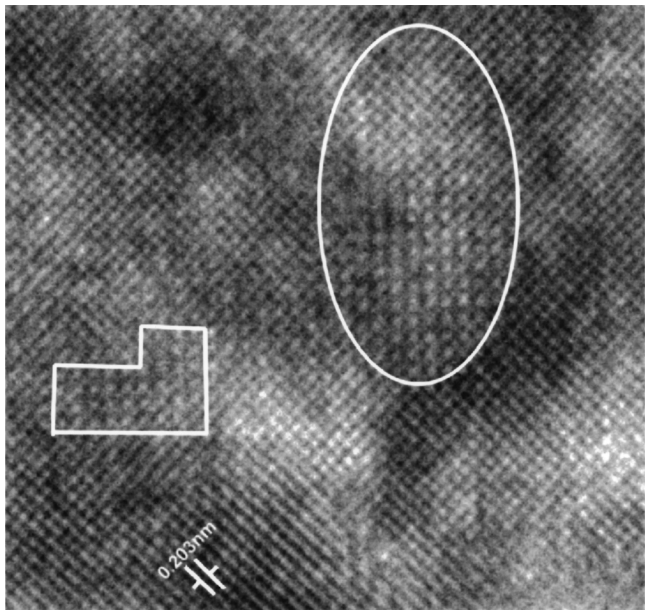

Fig. 3—HRTEM image of TiN precipitates in the αFe matrix. The sample was α-nitrided at 400 °C, 2 h and then reduced at 600 °C, 5 hours. The background is due to the fringes of {110} αFe planes within [001]-pole image. The precipitates are of intermediate size and follow the Bain OR. Note that the thickness and the width of the precipitates are comparable.

becomes too small to be observed. The TEM observations of the various stages of precipitate formation can be summarized as follows.

Streaking in FeNiCr samples was observed after 24 hours of nitriding at 400 °C (Figure 1(a)). At shorter times or lower

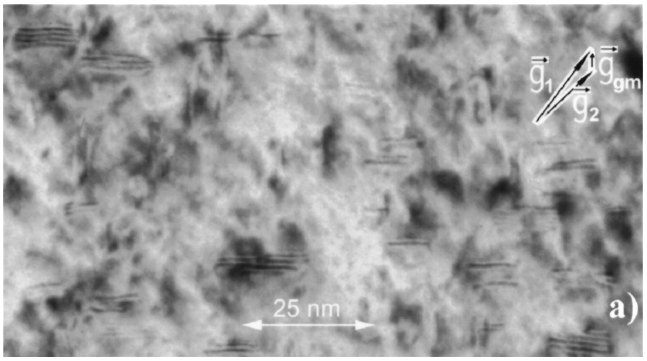

(*a*)

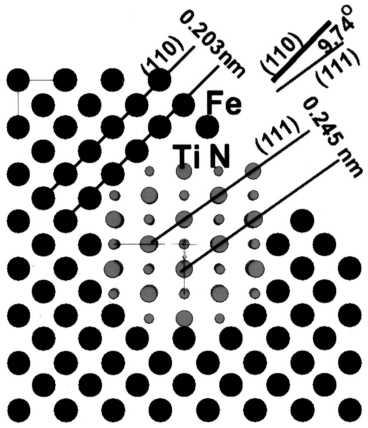

(*b*)

Fig. 4—(*a*) DF image, taken with $\mathbf{g}_2 = \mathbf{g}_{(110)\alpha Fe}$ in the [001]-zone area of a FeNiTiN sample, showing parallel fringes. The sample was α nitrided {400 °C, 1 h, $R_N = -6.8$} and then reduced {700 °C, 2 h, pure H_2}. (*b*) A schematic drawing of TiN precipitate in the α-Fe matrix, illustrating the origin of the moiré effect.

temperatures, the streaks are too faint to be observed, while at 400 °C and $t = 42$ hours, the streaking was already quite intense. At 500 °C, the streaking was observed after 1-hour α nitriding (Figure 4(b) in Reference 23), and after 2 hours, it was present all through the DP (Figure 1(b)).

Figure 1(c) illustrates that the streaking in the case of FeNiCr samples is relatively strong, *i.e.*, even in areas with multiple crystallite orientations. The sample was nitrided at 600 °C for 1 hour. The DPs are shown for an area containing three major crystallites with [001] orientation, slightly rotated with respect to each other. As discussed in Section IV, the fact that the streaking is pronounced and strictly follows the crystallite orientation proves that, at the given conditions in the Cr-containing alloys, the precipitates still form as thin platelets in the grain interiors and not (only) at grain boundaries.

Further, a more careful inspection of the streaks in Figure 1(c) showed that the smooth variation of the streak intensity is peaked not in {200}αFe spots, as in Figures 1(a) and (b), but at positions that correspond to {200} reflections for the CrN lattice. We conclude that platelets in the sample nitrided at 600 °C for 1 hour are thick enough to start producing their own {200} CrN reflections, though still too thin to generate sharp spots. From the length of the streaks, we estimate the average thickness to be $h \approx 6d_{\{200\}CrN} \approx 1.2$ nm under these nitriding conditions.

The streaking in FeNiTi samples appeared at lower temperature/shorter time conditions than in the FeNiCr case (Figures 2(a) and (b)). Faint traces of diffused streaking were observed even at $T = 300$ °C and $t = 1$ hour. Surprisingly, the streaks were usually much less intense (Figures 2(c) and 1(a)). Even at 500 °C (Figure 2(d)), the streaking in FeNiTi samples was relatively faint. The lower temperature/shorter time onset of precipitate formation for TiN, as compared to CrN, correlates with the larger (negative) free energy of TiN formation. However, the diffuseness of the streaking caused by TiN precipitates is not what one would expect. It is also interesting to note that, after reduction in a hydrogen atmosphere at 600 °C, the streaking becomes sharper (compare Figures 2(a) and (d)). The appearance of the streaks is analyzed in the Appendix. From the width of the streaks, we conclude that the TiN precipitates are small particles 0.2- to 0.3-nm thick and 1.5-nm wide, *i.e.*, containing only ~30 to 50 Ti sites. This is in accordance with Reference 6, who also estimated about 50 TiN molecules per platelet. The CrN precipitates are also platelets of a thickness between 0.2 and 1.2-nm thick, depending on the treatment, but with larger lateral dimensions because they produce narrow streaks. In Section IV, we argue that these observations indicate a difference in the kinetics of precipitate formation, leading to a different shape and size of the TiN and CrN precipitates.

Direct observation of thin platelets in HRTEM as coherent or semicoherent particles is difficult for several reasons: (1) a small size, (2) a small misfit in the major interface plane (Table I), (3) a large concentration of residual defects, (4) a small difference in atomic mass compared to the matrix, and (5) interference with an Fe_3O_4 oxide layer at the surface. Imaging of a precipitate with HRTEM has already been demonstrated for a CrN precipitate, oriented with its habit (100)CrN plane parallel to the (100)α-Fe plane and (011)CrN//(001)α-Fe normal to the electron-beam direction.[23] In Figure 3, a HRTEM image is shown for a nitrided and reduced FeNiTi sample (400 °C, 2 hours, $R_N = -6.8 +$ 600 °C, 5 hours, H_2). The overall feature of the figure is the fringes of the {110} αFe planes seen in the [001] orientation, which compose the background of the figure. The areas marked by white lines contain particles, which were ascribed to TiN precipitates with intermediate lateral dimensions (1.5×5 nm for the largest one), oriented with the (001) αFe/TiN interface plane normal to the electron-beam direction. The continuity of the {110} fringes suggests that the precipitates are coherent. However, the structure inside and around the precipitate is distorted. By its upper left corner, the largest precipitate is attached (pinned) to a large defect. Though the shape of the precipitate is difficult to define because of the diffuseness of the boundary, it is evident that its thickness and the width (both in the plane of the image) are comparable.

Reduction of the nitrided samples leads to a (partial) removal of the nitrogen from the matrix, whereas the nitrogen in the precipitates of the alloying element remains. This may result in a loss of coherency between the matrix and precipitates and in a relaxation of misfit stress. Such a relaxation favors the observation of precipitates, using moiré patterns. The loss of coherency is enhanced at higher annealing temperatures when the small TiN precipitates grow in size. In Figure 4(a), a dark-field micrograph is shown, taken

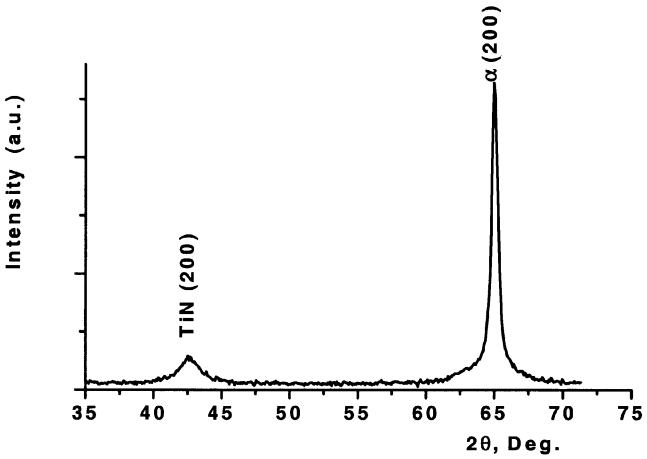

Fig. 5—XRD spectra for the Ti-containing alloy α nitrided at 500 °C and annealed at 1000 °C in vacuum. Note the 3-D TiN precipitate reflection.

with $\mathbf{g}_{(110)\alpha Fe}$ at 10^5 (100 k) magnification of an area with a [001] zone axis in a sample which was α nitrided (400 °C, 1 hour, $R_N = -6.8$) and then reduced at the relatively high temperature of 700 °C for 2 hours in pure H_2. The TiN precipitates are observed as parallel moiré fringes, indicating a preferred orientation with respect to the α-Fe matrix. The periodicity of the moiré fringes was 0.9 nm. At a higher magnification of 500 k, a HRTEM pattern (not shown) of this same sample clearly demonstrated the (110) planes of α-Fe, similar to the fringes in Figure 3. Direct comparison of the 100 and 500K images indicated that the moiré fringes were rotated over an angle of 36 deg with respect to the α-Fe (110) plane fringes, which can be explained as follows. We expect that TiN precipitates are arranged according to the Bain OR (Table I). In the schematic drawing of Figure 4(b), the beam direction, **B**, is parallel to the [001] direction of the α-Fe matrix. The platelets can grow with their interface plane either parallel or perpendicular to **B**. In the former case, the beam is, for example, parallel to the $[\bar{1}01]$ direction in the TiN precipitate. In this geometry, the (110) plane of the matrix with a d spacing of 0.203 nm makes an angle of 9.74 deg with the (111) plane of the precipitate with a d spacing of 0.245 nm. Moiré fringes are determined by the reciprocal vectors, $\mathbf{g_1}$ (110 α-Fe) and $\mathbf{g_2}$ (111 TiN) the spacing is $d_M = 1/|\mathbf{g_1} - \mathbf{g_2}|$, and the angle of rotation is $\gamma = \sin^{-1}(\sin\alpha\, g_2/|\mathbf{g_1} - \mathbf{g_2}|)$. The calculated values of the fringe distance and the rotation angle, $d_M = 0.88$ nm and $\gamma = 37.7$ deg, are in a good agreement with the experimental observations, which proves that the observed moiré fringes are indeed caused by the presence of precipitates with the lattice parameter of bulk TiN and with their planes parallel to the beam, *i.e.*, perpendicular to the surface.

The number of fringes is determined by the thickness of the precipitates; their length is given by the lateral size. Most of the precipitates give 1 to 2 fringes, though some have as many as 4 to 5. Their mean length is about 15 nm. From these observations, we estimate an average size of about 2 nm by 15 nm (or 2×15 nm^2).

At even higher temperature, noncoherent precipitates can attain sizes sufficient to produce reflections observable in XRD. An example is shown in Figure 5 for a Ti-containing alloy annealed at 1000 °C in vacuum, where the (002) reflection of TiN precipitates is observed. Using the Scherrer

relation,[24] the precipitate size is estimated to be 7 nm. It is noteworthy that the only TiN reflection appearing is (002) parallel to the (002) of the Fe matrix. In line with the Bain OR, we can conclude that three-dimensional (3-D) TiN precipitates prefer to grow with the (001) TiN/αFe interface plane parallel to the surface. It is in accordance with the HRTEM image (Figure 3), where the sample was reduced at lower temperature (600 °C). This is not always so for smaller precipitates, as evidenced by Figures 1 and 2. In this case, the appearance of the streaks proves that the plane of the coherent interface {100} (Ti/Cr)N is oriented perpendicular to the surface. This point is also illustrated by Figure 4 for a sample reduced at 700 °C. In addition, it is worthwhile to note that annealing at 1000 °C of pure Fe implies the $\alpha \rightarrow \gamma \rightarrow \alpha$ transitions (the transition temperature is 912 °C). In principle, such a phase cycling could lead to a change in the texture. However, we did not observe a change of texture.

Besides a number of irregular spots sometimes observable in the DPs and loosely referred to as misoriented small crystallites (for example, Figure 1(d)), there are also extra spots, which appear regularly in the DP (Figures 1 and 2). Among them are forbidden {100} reflections and cross-like satellites (x satellites) around {110} spots, which could be approximately indexed as {1 ± 1/2, 1, 0} and {1, 1 ± 1/2, 0} (Figures 2(b) and (d)). Because the {100} spots and x satellites were also observed on pure unnitrided Fe samples, the extra spots cannot be due to any nitride. It is highly probable that this is caused by rel-rod effects[25] of a thin outermost oxide layer of fcc Fe_3O_4, as has already been discussed in the literature.[26,27] The oxide layer is coherent with the (001) Fe surface with a Bain-type OR: (001)bcc// (001)fcc and [100]bcc//[110]fcc. The mismatch at the (001) interface α-Fe/Fe_3O_4, $\varepsilon = (8.35 \times \sqrt{2} - 4 \times 2.87)/4 \times 2.87 \approx 0.029$, is small, and this makes direct identification of the oxide layer in a DP rather difficult, but sometimes thin oxide layers show up as rel-rod effects (Figures 1 and 2). The apparent {100} spots then represent {220} Fe_3O_4, and the x satellites are rods of {311} Fe_3O_4 and {131} Fe_3O_4, which intersect the Ewald sphere when the oxide layer is thin enough.

B. *Initial Stage of Formation of Precipitates*

As demonstrated in References 28 and 23, the formation of precipitates can be followed with MS techniques. Besides the typical α-Fe matrix Mössbauer sextet for as-rolled material, extra components appear corresponding to first and second nearest-neighbor nonmagnetic Ti/Cr atoms. After nitriding, these components are broadened, indicating a variety of nonmagnetic atoms around Fe atoms. Typical MS spectra are shown in Figures 6 and 7 for a Ti- and a Cr-containing alloy, respectively.

In FeNiTi foils after cold rolling (Figure 6(a)), the spectra can be fitted by two components: component (1) corresponds to matrix atoms considered as a mixture of Fe and Ni atoms, and component (2) corresponds to iron atoms having one Ti neighbor in the first or second coordination shells.[28] The Ti-atomic component disappears very soon after nitriding. An example is shown in the spectrum of Figure 6(b) for a sample nitrided at 400 °C and $t = 1$ hour, where the Ti neighbor satellite is replaced by a broader component (2) given by iron atoms with different environments: N atoms and TiN precipitates. In the MS spectrum (c), one can see

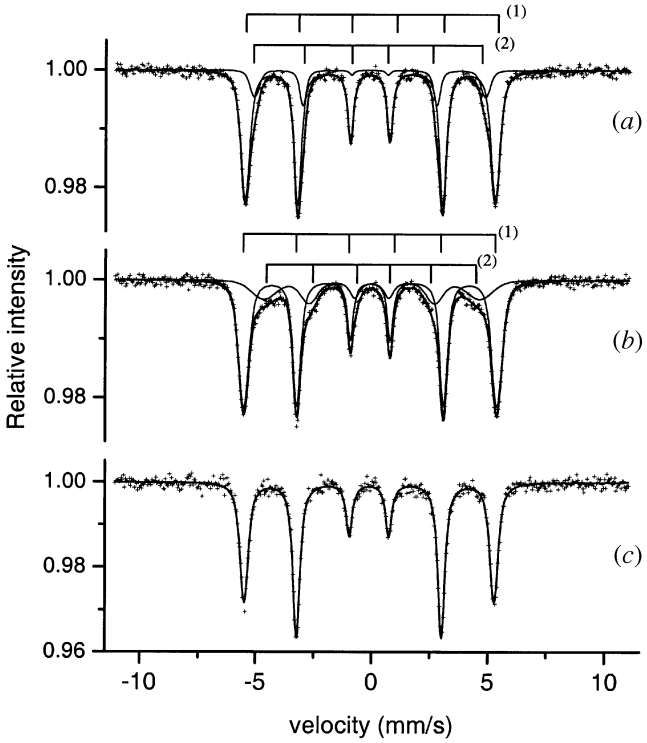

Fig. 6—(*a*) MS spectrum of the Ti-containing alloy after cold rolling: component (1) corresponds to matrix atoms considered as a mixture of Fe and Ni atoms, and component (2) corresponds to iron atoms having one Ti atom in the first two coordination shells. (*b*) After α nitriding at 400 °C, the Ti neighbor satellite is replaced by a broader component (2) caused by iron atoms with different environments: N and TiN precipitates. (*c*) MS spectrum after 2 h reducing at 700 °C in dry H2. Only the iron sextet is visible, suggesting that bigger precipitates have been formed.

that after 2 hours reduction at 700 °C in a dry H_2 atmosphere, only the iron sextet is visible, indicating that bigger precipitates have grown, and the relative number of nonferromagnetic neighbors is decreased to less than 0.5 pct.

In the MS spectrum of an FeNiCr alloy after cold rolling (Figure 7(a)), three components could be distinguished: component (1), as for the FeNiTi alloy, is due to the matrix atoms (Fe + Ni), and components (2) and (3) correspond to iron atoms having, respectively, one and two Cr atoms in the first two coordination shells. After nitriding at 400 °C and $t = 24$ hours, the spectrum of Figure 7(b), the contribution of atomically dissolved Cr in component (2) decreased but is still significant, in contrast to the nitrided Ti-containing alloy. Component (3) is slightly shifted in the spectrum of Figure 7(b) with respect to component (3) in Figure 7(a) and corresponds to iron atoms with different environments, containing N. The extra components become invisible after nitriding at 600 °C.

From the MS spectra, the concentration of Fe atoms having Ti and Cr neighbors can be estimated.[28] This leads to an estimate of the atomically dissolved fractions of Ti and Cr. In as-rolled material, these atomic fractions are 1.4 and 2.8 at. pct, respectively, for Ti and Cr. Evidently, the rest of the components (0.5 at. pct Ti and 0.2 at. pct Cr) are not atomically dissolved and are probably present in small clusters. As has been mentioned already, the Ti-atomic component becomes negligibly small after nitriding of FeNiTi alloy; for the Cr-containing alloy, some of the data are presented in the fourth column of Table II.

In Figure 8, the data for the Ti-containing sample on the intensity of the MS component, shifted because of the presence of nitrogen, is plotted *vs* the excess-nitrogen content. As follows from the discussion, this data gives evidence that most of the excess nitrogen is dissolved in the matrix.

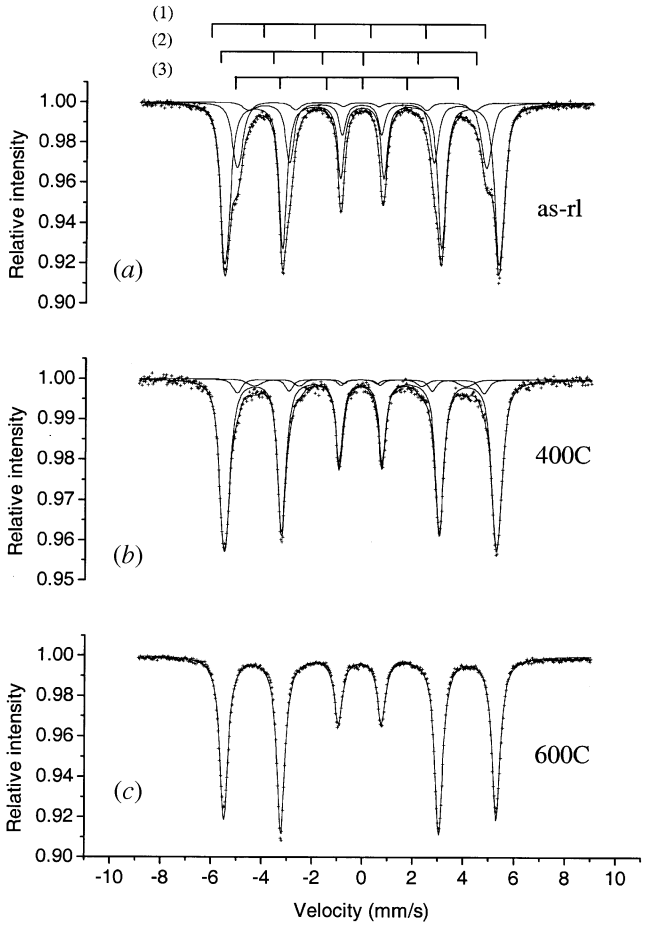

Fig. 7—(*a*) MS spectrum of the Cr-containing alloy after cold rolling: component (1) corresponds to matrix atoms considered as a mixture of Fe and Ni atoms, and components (2) and (3) correspond to iron atoms having one Cr and two Cr atoms in the first two coordination shells, respectively. (*b*) After α nitriding at 400 °C, there is still intensity left from metallic Cr atoms in component (2). Component (3) is given by iron atoms with a different environments containing N. (*c*) MS spectrum after nitriding at 600 °C.

C. *Nitrogen Content and Matrix Dilation*

Only a small amount of nitrogen can be dissolved in the pure αFe matrix (0.23 at. pct at 500 °C[29]). The major fraction of nitrogen absorbed by the alloy is connected with the formation of precipitates of alloying elements and with the influence of the alloying elements and their precipitates on the matrix. The nitrogen uptake in $Fe_{93}Ni_4Cr_3$ and in $Fe_{94}Ni_4Ti_2$ foils, as obtained by weighing the samples, is shown in the third column of Tables II and III, respectively. Often, we observed a variation of the nitrogen uptake for the same nitriding conditions, especially for a short time of nitriding; the scatter being larger than possible errors in the weighing procedure. Also, we cannot ascribe this scatter to an uncertainty in the nitriding conditions because these were well controlled. Although not completely established, we believe that it is connected with a different arrangement/density of defects in different samples after cold rolling. Although the plastic flow during rolling was evidently by excitation of multiple slip directions, the actual distribution of these modes can be expected to be different in different areas (say, in the center and at the edge) of a foil under deformation. This conclusion is in agreement with a variation of strains revealed by XRD in as-rolled films. The defect configuration and density influence the kinetics of formation of the precipitates and, hence, the shape of precipitates and

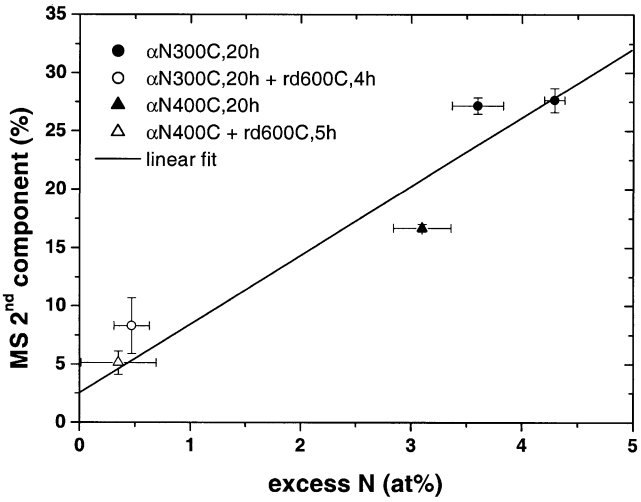

Fig. 8—Intensity of MS second component *vs* $[N]_{ex}$ for the Ti-containing alloy.

Table II. Nitrogen Uptake in the $Fe_{93}Ni_4Cr_3$ Foils and the Lattice Parameter of the Bcc Matrix

Sample	Treatment*	[N], At. Pct	$[Cr]_{at}$, At. Pct**	$[N]_{ex}$, At. Pct†	*a* (Shift), nm‡	*a* (Unshift), nm§
As-rolled	as-rolled	0	2.8	0	0.2873	0.2873
Cr1	300 °C, 50 h, −5.55	0.66	2.7	0.5	0.2873	0.2873
Cr2	400 °C, 24 h, −6.5	3.26	0.5	0.9	0.2891	0.2876
Cr3	500 °C, 1 h, −7.34	4.28	0	1.6	0.2892	0.2876
Cr4	550 °C, 1.3 h, −7.62	3.25	0	0.5	0.2892	0.2872
Cr5	600 °C, 0.5 h, −8.06	2.99	0	0.3	0.2872	0.2872

*Indicated are temperature, treatment time, R_N.
**Concentration of atomically dissolved Cr, estimated from MS spectra.
†Concentration of excess nitrogen, estimated with the correction included for "free" Cr atoms, Eq. [2].
‡Lattice parameters of the bcc matrix, obtained from the shifted component of the (222) bcc line.
§Lattice parameter from the unshifted component.

Table III. Nitrogen Uptake in the $Fe_{94}Ni_4Ti_2$ Foils and the Lattice Parameter of the Bcc Matrix

Sample	Treatment*	[N], At. Pct	$[N]_{ex}$, At. Pct	*a*, nm**
Ti0	as-rolled	0	0	0.2880
	Short Nitriding			
Tia	300 °C, 2 h, −5.1	6.56	4.7	0.2926
Tib	300 °C, 2 h, −5.1	5.50	3.6	—
Tii	400 °C, 2 h, −6.2	7.10	5.2	0.2922
Tij	400 °C, 2 h, −6.2	6.30	4.4	—
Tik	500 °C, 2 h, −7.1	5.70	3.8	0.2912
Til	500 °C, 2 h, −7.1	4.80	2.9	—
	Long Nitriding			
Ti10	as-rolled	0	0	0.2877
Ti20	as-rolled	0	0	0.2876
Ti2	300 °C, 20 h, −5.0	6.43	4.6	—
Ti3	300 °C, 20 h, −5.0	6.19	4.3	0.2936
Ti4	300 °C, 20 h, −5.0	5.50	3.6	0.2919
Ti5	400 °C, 20 h, −6.8	5.00	3.1	0.2913
	Reduction			
Ti2r	Ti2 + 600 °C, 4 h, H2	2.37	0.4	0.2892
Ti5r	Ti5 + 600 °C, 5 h, H2	2.25	0.3	0.2893

*Indicated are temperature, treatment time, R_N, if not H_2 atmosphere.

**Lattice constants calculated from the peak position of the main (002) diffracted K_α line.

the total amount of nitrogen absorbed, as we will see in Discussion. Whatever the reason is, the uncertainty in total nitrogen uptake does not influence our conclusions.

The nitrogen concentration, $[N]_{ex}$, in excess of the concentration required for the stoichiometric MN compound is normally called "excess nitrogen," *i.e.*,

$$[N]_{ex} \equiv [N] - [N]_{MN} - [N]_\alpha{}^0 \qquad [1]$$

where [N], $[N]_{MN}$, and $[N]_\alpha{}^0$ stand for fractions of, respectively, total, stoichiometric equilibrium nitride, and nitrogen equilibrium solubility of pure iron under identical nitriding conditions.[5,15,17] Note that "concentration" in this article is defined as the relative fraction of a species with respect to all atoms, including Ni, and Ti or Cr, N, and Fe. The $[N]_{MN}$ is estimated from the concentration of the alloying metal in the material, assuming a 1:1 stoichiometric ratio of the MN precipitate. But if "free" M atoms are present, as in the Cr-containing alloy, the notion of excess nitrogen requires a correction. According to MS data, a large free or atomically dispersed fraction $[Cr]_{at}$ exists at 300 °C and $t = 50$ hours, and about 18 pct of all Cr atoms are still in solution at 400 °C and $t = 24$ hours (column 4 in Table II). The fraction of N, bound by the alloying element, is smaller when atomically dissolved metal is still present to a concentration $[M]_{at}$:

$$[N]_{MN} = [M]^0 - [M]_{at} \qquad [2]$$

Here, $[M]^0$ is the total concentration of the alloying element. The amount of $[N]_{ex}$, determined with the correction of Eq. [2] in the Cr-containing alloy, is listed in column 5 of Table II. For the Ti-containing alloy the "free-atom" correction is not required because there was no free Ti-atom fraction observed after nitriding. The estimated error in $[N]_{ex}$ is about 0.25 at. pct.

From a comparison of the data in third column of Tables II and III, one can conclude that the ratio of the nitrogen to chromium concentrations, [N]/[Cr], is not much larger than unity, while the [N]/[Ti] ratio for nitrided samples is normally much higher than unity, indicating a large fraction of excess nitrogen in this case. An intriguing point is that the N content, column 3 in Table III, is decreasing after nitriding the Ti foils at temperatures $T > 400$ °C. We come back to this point in the following paragraph in connection with XRD data.

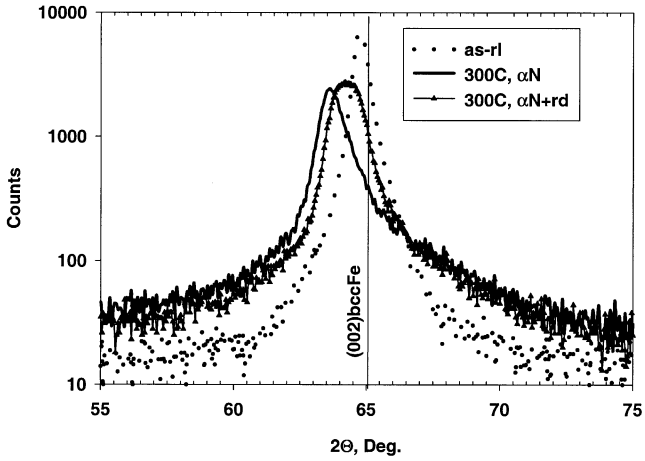

Fig. 9—XRD θ-2θ scans for the as-rolled, α-nitrided (300 °C, 2 h), and reduced (300 °C, 2 h) Ti-containing alloy in the vicinity of the (002)αFe line (shown by a vertical line).

With one-dimensional ϑ-2ϑ, as well as with two-dimensional (2-D) texture XRD scans, we observed that, in the as-rolled foils, the (001) texture was dominating with some mixture of (111) texture. As examples, XRD spectra in the region of the αFe (002) reflection are shown in Figure 9 for $Fe_{94}Ni_4Ti_2$ samples as-rolled, nitrided, and nitrided and then reduced (300 °C and 2 hours for all treatments). Similarly, in Figure 10, spectra are shown in the region of the αFe (222) reflection for $Fe_{93}Ni_4Cr_3$ samples nitrided at different temperatures. Because of the presence of the alloying Ni and Ti/Cr elements, the XRD lines for the as-rolled foils are shifted with respect to the positions of the XRD lines for αFe. For the Ti-containing alloy, the observed lattice parameter is $a = 0.2877(2)$ nm, which is ≈0.4 pct larger than the value $a = 0.2866$ nm for pure αFe, while, for the Cr-containing alloy, $a = 0.2871$ nm was only ~0.13 pct larger than for pure αFe. Such a difference cannot be substantiated by Vegard's law. Evidently, the effect is due to a difference in the degree of dissimilarity (electron-shell configuration, ionic radii, r(Ti) = 0.146 nm, and r(Cr) = 0.126 nm) of Ti and Cr compared to Fe (r(Fe) = 0.127 nm), causing larger strains in the Ti-containing alloy foils after rolling. From Figures 9 and 10, one can see that nitriding in the α region has a twofold effect on the matrix: a shift of the XRD lines to lower diffraction angles, indicating an overall dilation of the bcc Fe-lattice, and a change in the line shape, pointing to a local variation in the microstructure or the strain/stress state in the foils. In Figure 10, the lines were fitted with two Lorentzian components. Each component contains contributions caused by diffraction of the Cu $K_{\alpha1}$ and $K_{\alpha2}$ lines.

The variation of the lattice parameter for the nitrided Ti alloy *vs* the excess-nitrogen content, $a([N]_{ex})$, is plotted in Figure 11. The lattice parameter was calculated from the position of the peak of the (002) bcc reflection. As one can

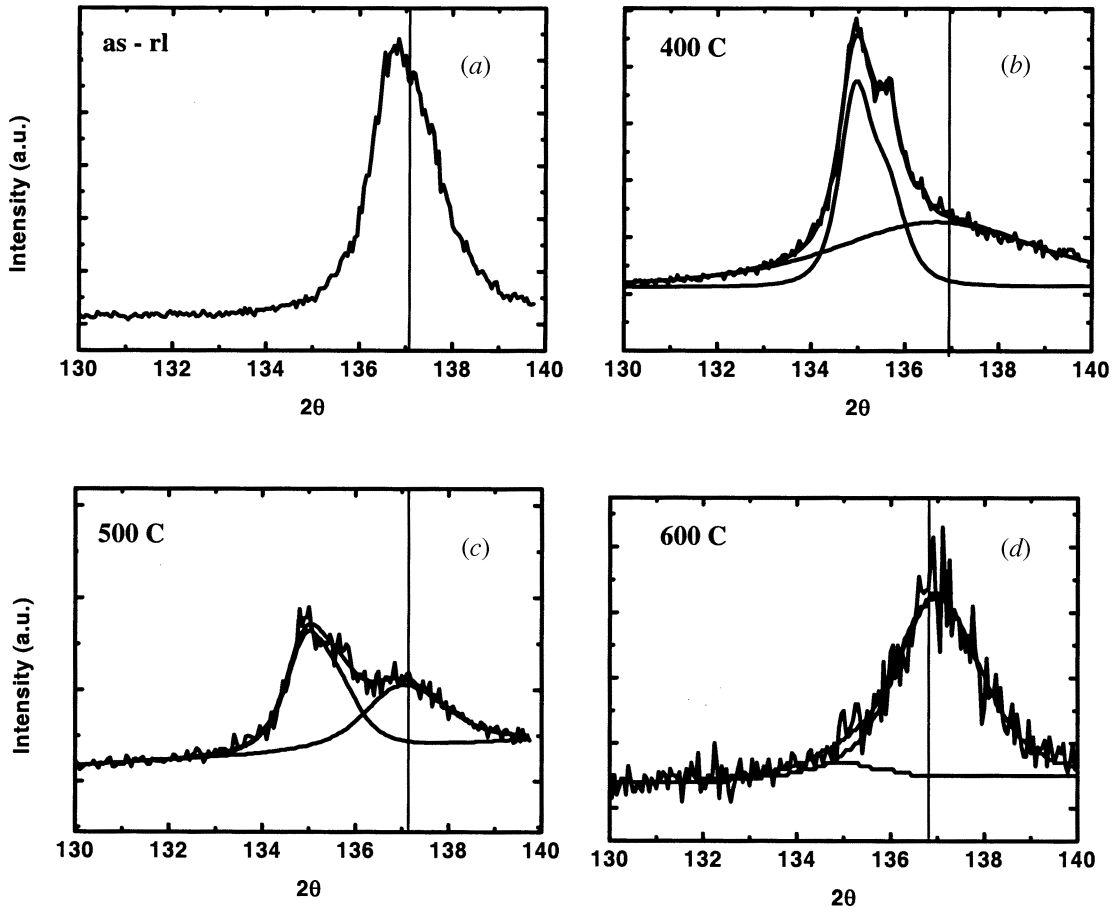

Fig. 10—XRD scans for the Cr-containing alloy in the vicinity of (222)αFe (shown by vertical lines): (*a*) as-rolled; (*b*) nitrided at 400 °C, 24 h, and $R_N = -6.5$; (*c*) nitrided at 500 °C, 1 h, and $R_N = -7.34$; and (*d*) nitrided at 600 °C, 0.5 h, and $R_N = -8.06$. The spectra are fitted with two components: the strained component, shifted with respect to the (222)αFe line, and the second, almost unshifted (unstrained), component in (b) and (c) pointing to a nonuniform deformation of the lattice.

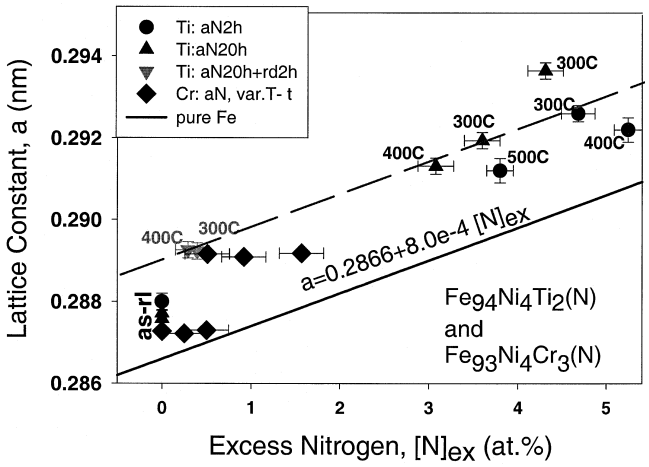

Fig. 11—Variation of the lattice parameter of the Ti-containing and Cr-containing alloys as a function of excess nitrogen content. By a solid straight line is shown the dependence for nitrided pure iron.[29,38] A dashed straight line is drawn through the data points parallel to the solid line to guide the eye.

conclude from Table III and Figure 11, nitriding at higher temperature or time does not necessarily lead to higher nitrogen content or higher lattice dilation. For example, after nitriding for 2 hours at 300 °C, the nitrogen uptake is larger than at 500 °C. Similar observations can be made for prolonged (20 hours) nitriding at 300 °C and 400 °C. These results are in accordance with those reported by Jack,[5] although an explanation was missing. In our case, the nitrogen potential was chosen to be within the α region for the Fe-N system. So, it is different for different temperatures. We choose our R_N values, $R_N = -5.0$ (300 °C) and $R_N = -6.8$ (400 °C), close to the saturation values as follows from References 5 and 8. In Reference 5, the saturation level in [N] *vs* R_N dependence was higher in the sequence 550 °C, 500 °C, and 300 °C. Thus, not the difference in R_N, but the mechanism of TiN-precipitate formation and the interaction of precipitates with the matrix are responsible for the unexpected temperature variation in the lattice parameters and nitrogen uptake. In Section IV, we argue that an increase in the thickness or lateral size of the platelets both lead to a lower excess-N content.

After reduction of the nitrided Ti-containing samples in an H_2 atmosphere, the lattice parameter becomes smaller than for a nitrided sample, but it is still higher than that of the as-rolled material. This residual expansion of the matrix can be due to strain induced by a residual semicoherency of finely dispersed precipitates. As the TiN precipitates coarsen,

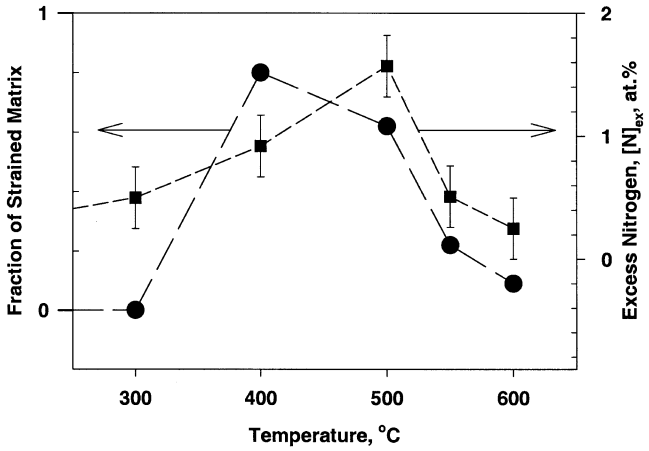

Fig. 12—Variation of the fraction of the strained component and the excess nitrogen content with temperature of nitriding for the Cr-containing alloy.

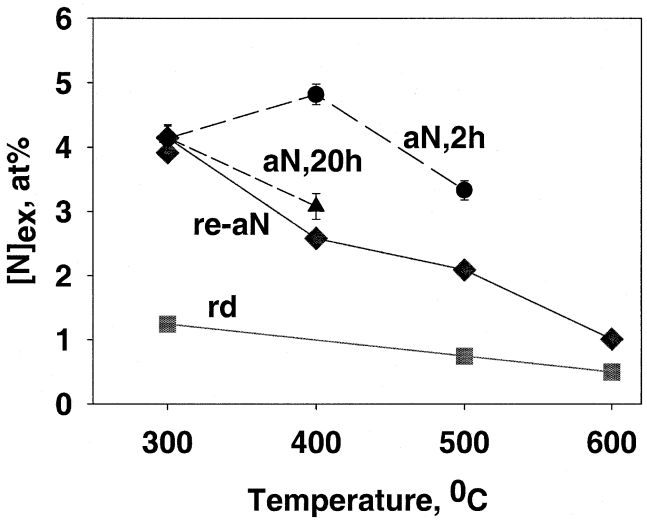

Fig. 13—Excess nitrogen content in Ti-containing alloy *vs* temperature of the reduced (rd, squares) and re-nitrided (re-aN, diamonds). Note, that at T = 300 °C, the lower point corresponds to as-nitrided samples; after reduction and renitriding at the same temperature, the amount of nitrogen is completely restored. For comparison, the data for α-nitriding during 20 h (aN, 20 h, triangles) and 2 h (aN, 2 h, circles) are also shown. At T = 300 °C, these data coincide.

their influence upon the matrix diminishes, and the lattice parameter of the ferrite decreases to 0.287 nm (approximately equal to the lattice parameter of αFe) after reduction at 700 °C.

For the nitrided Cr-containing alloy, the lattice constants, listed in Table II, were obtained by fitting of the (222) bcc lines (Figure 10) by two components. One of them is shifted to lower 2ϑ values, pointing to a local dilation of the matrix, while the second line stays at the almost unshifted (222) αFe position, indicating the presence of an unstrained fraction even at the highest nitrogen content in the alloy. The values of the lattice parameters of shifted and unshifted components are listed in the columns 6 and 7 of Table II. The variation of the lattice constant as derived from the position of the shifted component as a function of total nitrogen content is depicted in Figure 11. One can see that the expansion of the matrix in the nitrided Cr-containing alloy is much less than in the Ti-containing alloy. From Table II and from Figures 10 and 11, it is also clear that the variation of the lattice constants of the strained and unstrained components with the temperature is not very large (in contrast with the Ti-containing alloy), but the relative intensity of the strained component strongly depends on the temperature of nitriding (Figure 12). The strained component is negligibly small after the nitriding at 300 °C; at 400 °C, it clearly dominates, and it diminishes again after nitriding at 600 °C. The variation of the strained component fraction with temperature correlates with the similar behavior of the excess-nitrogen uptake, as is observed in Figure 12.

D. *Nitrogen Content in Reduced and Renitrided FeTi Samples*

A common statement in literature is that annealing in a hydrogen atmosphere reduces the nitrogen content to a concentration, corresponding to the 1:1 stoichiometric composition of the alloying element nitride.[5,6,15] Another common statement is that the reduction is reversible, *i.e.*, renitriding restores the initial nitrogen content present prior the reduction, *i.e.*, Reference 5. We will show that both statements are not in agreement with our observations for Ti-containing foils. We performed a study of the nitrogen content after reduction and renitriding of Ti-containing foils as a function of the processing temperature. Four samples were nitrided, reduced, and renitrided at the same temperature. This was done at four different temperatures. The nitrogen content in the samples was determined by weighing with a microbalance. The results are plotted in Figure 13, where each point is an average over the data of the four samples. The time of the treatment at each step was about 20 hours. As one can see, the excess-nitrogen content is the highest after renitriding at 300 °C, higher than 4 at. pct, being about the same as for the first nitriding at this temperature. The data shows that the higher the temperature of the treatment is, the smaller the amount of nitrogen that is taken up again after renitriding of a reduced sample. Also, the excess nitrogen does not vanish after reduction in an H_2 atmosphere, but the residual amount of $[N]_{ex}$ decreases from more than 1 at. pct at T = 300 °C to ~0.5 at. pct at T = 600 °C.

For the sake of comparison, Figure 13 also displays the data for short (2 hours) and prolonged (20 hours) nitriding from Table III, averaged for the given temperature. Note, that, at T = 300 °C, the points of three data sets cannot be distinguished. One can see that, while the prolonged nitriding data follows the trend of the renitriding data, the data for short nitriding deviate significantly.

IV. DISCUSSION

We summarize the main observations relevant for the discussion as follows.

(1) Streaking along {200} in the nitrided Ti-containing alloy starts at a lower temperature and occurs at shorter time ($T - t$), compared with the Cr alloy, but the streaks are more diffuse (Figures 1 and 2).
(2) With increasing time or temperature (up to 500 °C was applied) of nitriding, the width of the streaks in the Ti-containing alloy does not change drastically. Reduction

at 600 °C makes the streaks more narrow and sharp (Figure 2).

(3) After reduction at 700 °C and higher, the TiN precipitates grow large enough to produce moiré fringes in TEM (Figure 4(a)). The XRD lines of TiN can be observed after annealing at 1000 °C (Figure 5). The lattice constant of the matrix approaches the value for pure αFe.

(4) The Ti-atom component in the MS spectra disappears at low temperatures and time ($T - t$), while the Cr-atom component is still prominent, up to the relatively high temperature of 400 °C, compare Figures 6 and 7.

(5) Sharp streaking in the Cr-containing alloy is observable after nitriding at temperatures up to 600 °C. It is also observed in the areas with small grains. Streaking follows the local grain orientation.

(6) The amount of nitrogen absorbed and the matrix expansion are much larger in the Ti-containing alloy than in the Cr alloy (Tables II and III and Figure 11).

(7) The higher the temperature of the treatment is, the smaller the amount of nitrogen that is taken up again after renitriding of a reduced sample. Some excess nitrogen is left in the FeNiTiN alloy after reduction in an H_2 atmosphere at temperatures below 600 °C (Figure 12).

(8) The intensity of the second component in the MS spectra increases with an increase of excess nitrogen (Figure 8).

(9) The XRD lines of nitrided Ti- and Cr-containing alloys can be approximated by two components, reflecting a strained and an unstrained state of the matrix. The variation of the dilation of the matrix with nitriding temperature for the Cr alloy was weak, whereas in the Ti-containing alloy this dilation varies strongly with the nitriding temperature. In contrast to this, in the Cr-containing alloy, the variation of the fraction of the dilated component of the matrix strongly depends on the temperature; at $T_{\alpha N} = 600$ °C, the dilated component has almost vanished (Figures 11 and 12)

A. *Formation, Shape, and Size of TiN and CrN Precipitates*

The precipitate formation is determined by the change in the Gibbs free energies and by the mobility of the species. Here, we discuss the energetics of the formation of the TiN and CrN precipitates. The change in the Gibbs free energy upon formation of precipitates in a matrix includes, besides the chemical contribution, ΔG_{ch}, a strain term, ΔG_{str}, an interface term, ΔG_i, and a term ΔG_d, accounting for the presence of defects in the matrix, which makes the formation of the precipitates easier, *i.e.*,

$$\begin{aligned}\Delta G &= (\Delta G_{ch} + \Delta G_d) + \Delta G_{\text{str}} + \Delta G_i \\ &= -\Delta G_{\text{drive}} + \Delta G_{\text{str}} + \Delta G_i\end{aligned} \quad [3]$$

Both, ΔG_{ch} and ΔG_d, are negative, while ΔG_{str} and ΔG_i are positive. The chemical term is mainly determined by the enthalpy of MN formation; the entropy term being very small. The resulting Gibbs free energy is almost independent of temperature in the range of interest, and it is much higher for TiN than for CrN, as can be seen from Table IV, where in the second and third columns these values are listed, as estimated from Reference 30 and obtained by Reference 17, respectively.

Table IV. Gibbs Free Energies for TiN and CrN Precipitates

Precipitate	ΔG_{ch},* kJ/mol	ΔG_{ch},** kJ/mol	ΔG_{str},** kJ/mol
TiN	−336	−300	170
CrN	−125	−91	120

*Estimated from Ref. 30.
**Obtained by Ref. 17.

Estimates by Somers *et al.*[17] for the strain energies, considering an isotropic defectless αFe matrix with spherical noncompressible precipitates, are given in the fourth column of Table IV. It is evident that the assumptions are too rough because, for example, the formation of CrN precipitates in a crystal without defects would not be possible. More accurate estimates, which take into account the anisotropy of crystals, the compressibility of the precipitates, and the coherency according to the theory of Eshelby[31] and following researchers, *e.g.*, Reference 32, are to the best of our knowledge not available. Nevertheless, the data in Table IV illustrates that the variation of the chemical term is much stronger than the variation of the strain energy term for these two alloys.

By the additional negative term, ΔG_d, in Eq. [3], we account for all missing corrections that make the driving force, $\Delta G_{\text{drive}} = |\Delta G_{ch} + \Delta G_d|$, large enough to make precipitation favorable. The term ΔG_d is to a large extent determined by a reduction of the strain energy caused by the presence of a dislocation network. Assuming that the dislocation density is not very different for Cr- and Ti-containing foils, we can state that the driving energy for formation of TiN precipitates is much larger than that for CrN precipitates. This larger driving force can play an important role in the formation and evolution of the TiN precipitates and will affect the shape, coherency, and stability of the precipitates. Also, if a part of the Ti atoms in a cluster will be substituted by Fe atoms, as in Fe-Ti-N GP zones, thus reducing to some extent the ΔG_{ch} term and, hence, ΔG_{drive} in Eq. [3], the cluster can still be stable.

Observation (1) was analyzed in the Appendix, where we concluded that the TiN precipitates, formed during nitriding at 300 °C, are small particles 0.2- to 0.3-nm thick and 1.5-nm wide, *i.e.*, containing only ~30 to 50 Ti sites, in accordance with Reference 6, who also estimated about 50 TiN molecules per platelet. The CrN precipitates, formed at $T =$ 400 °C to 500 °C, are also platelets 0.2 to 1.2-nm thick, depending on the treatment, but with larger lateral dimension.

The fact that the precipitates are small implies that the spacing between them is also small. The distance between neighboring TiN clusters, formed at 300 °C and 21 hours, is $U^{1/3} = (2V/[\text{M}])^{1/3}\ (a_{\alpha\text{Fe}}/a_{\text{MN}}) \approx 2.5$ nm ($V \approx 0.5$ nm^3, $[\text{M}] = [\text{Ti}] = 0.02$, $a_{\alpha\text{Fe}} \approx 0.287$ nm, and $a_{\text{TiN}} = 0.424$ nm). For the formation of the observed precipitates, diffusion of Ti over only five interatomic distances would be required. The mobility of Ti in pure, defect-free Fe is too low[33] (by six orders of magnitude) to explain the precipitation even over such small distances. Because Ti is oversized with respect to Fe atoms (Section III–D), one may suppose that vacancies present in the defected material are trapped at Ti atoms. The mobility of such a vacancy-Ti complex would be sufficiently fast to explain the TiN precipitation at this

low temperature. This also will be true, if the vacancy is filled with an interstitial atom, such as N. The size of the TiN precipitates does not change significantly after treatments at 400 °C and 500 °C, compared with $T = 300$ °C (observation 2). This indicates that the high cohesion energy precludes Ti atoms or TiN molecules to desolve from TiN clusters (observation 4), thus hindering the ripening. At higher temperatures (600 °C and higher), the TiN precipitates start to grow and finally loose the coherency with the matrix, which leads to the moiré fringes in TEM and to the corresponding peak in XRD (Figures 4(a) and (5)).

The Cr-containing alloy behaves differently. Because Cr atoms are slightly undersized with respect to Fe atoms (Section III–D), no binding of vacancy with the Cr atom is to be expected. The precipitate formation is consistent with the diffusivity of Cr atoms in pure, defect-free Fe. There was no sign of CrN formation at $T = 300$ °C; hence, the diffusivity was too low at this temperature. At $T = 400$ °C, however, the CrN precipitates are already larger than the corresponding TiN precipitates, giving a lower limit of the diffusion coefficient, $D > 2 \times 10^{-18}$ cm^2/s, for Cr in the alloy. Using the activation energy, $Q = 56$ kcal/g at., and the pre-exponential factor, $D_0 = 7.6$ cm^2/s, from Reference 33 for Cr in pure Fe, one can estimate the diffusion coefficient, $D = 4.5 \times 10^{-21}$ and 5×10^{-18} cm^2/s for $T = 300$ °C and 400 °C, respectively, in agreement with the experimental observations. In contrast with TiN, at the periphery of a CrN precipitate, Cr and N atoms are in a dynamical equilibrium, permanently desolving and precipitating again (observation 4). A relatively weak driving force is required to dissociate a Cr atom (or a CrN molecule) from a small CrN precipitate, leading to a larger precipitate.

B. *Location of the Precipitates*

There is no evidence that TiN precipitates grow preferentially on grain boundaries at all regimes investigated. The reasons for this were discussed previously. The situation is quite different for CrN precipitates. Preferential growth at grain boundaries (discontinuous precipitation) was reported in the literature[34,18] and in Reference 3. One could make a similar conclusion from the observations reported in Reference 35. Because we have evidence of strong streaking in a multicrystalline area of the Cr-containing sample after nitriding at 600 °C and 1 hour, where the streaks follow the crystallite orientation, (observation 5, Figure 1(c)), we can conclude that the growth at grain boundaries is not preferential in our case. As discussed by Nabarro,[36] the elastic-strain energy promotes the formation of disklike (2-D) precipitates. In contrast, there is a tendency to form a 3-D precipitate at the grain boundary. There the coherency with the matrix and, hence, the elastic-strain energy of a particle is reduced, while the interface energy of the particle is increased. The shape of the particle is determined by the tendency to minimize ΔG_i in Eq. [3].[37] Thus, there would be no streaking in the case of grain-boundary precipitates, contrary to our observation. The formation of CrN precipitates at the grain boundaries reported in References 17, 3, 34, and 18 is most probably connected with a low density and a low pinning energy, *i.e.*, ΔG_d in Eq. [3], of the defects, for CrN in the bulk or a relatively large nitriding time. Indeed, in these works, defects were only introduced during mechanical polishing. Sometimes their samples were annealed (850 °C and 18 hours[3]). Evidently, in our case, defects in the bulk of the crystallites serve as nucleation sites and pinning points for CrN precipitates because of the contribution of ΔG_d in Eq. [3]. Thus, a larger energy (temperature) is required to relocate the precipitate to the grain boundaries. Our result is consistent with the observation in Reference 7, where it was shown that cold working of the alloy prevents the formation of precipitates at the grain boundaries, which improves the mechanical properties of the nitrided Fe-Ti alloy.

C. *Matrix Dilation and Nitrogen Uptake*

According to observation 6, Tables II and III, and Figure 11, the lattice dilation and the nitrogen content is larger in the nitrided Ti-containing alloy than in the Cr-containing alloy. For example, the ratio $([N]/[Ti])_{max}$ is normally more than 3 for nitrided samples, while $([N]/[Cr])_{max}$ was at most 1.6. We relate the lattice dilation and the nitrogen content with the size and shape of the precipitates when the misfit is taken up by the elastically coherent interface between the precipitate and the matrix.

The lattice mismatch between the αFe matrix and a precipitate with the bulk TiN structure (Table I) and the Fe matrix is too large for coherency at the interface. On the other hand, without coherency, there would be no expansion of the matrix and only a very small amount of excess nitrogen would be taken up. This conclusion is based on observations of a reduction of the dilation of the matrix and the corresponding nitrogen content with coarsening of the precipitates (observations 2, 3, and 7). Coherency can be established if mixed (FeTi)N clusters are formed at low (300 °C) temperatures. The presence of Fe in the cluster reduces the mismatch and the elastic modulus, compared with pure TiN precipitates, making coherency more accessible. With an average distance between neighboring precipitates of about 3 nm and alignment of the platelets parallel to the cubic faces, the misfit-induced long-range strains in the matrix can easily overlap between the platelets, promoting the overall dilation. The large amount of the excess nitrogen observed for the nitrided Ti-containing alloy is then the result of, and not the cause for, the dilation. For platelets, which are wider by a factor of 10, the average distance between platelets becomes $\approx$14 nm. Evidently, in this case, the overlap is much less, and the unstrained component is more pronounced. This situation is observed for the nitrided Cr-containing samples and for Ti-containing samples nitrided and reduced at high temperatures (observation 9).

Our MS data for the Ti alloy presented in Figure 8, observation 8, give evidence that most of the excess nitrogen after nitriding at 300 °C, 20 hours, and $R_N = -5.0$ is randomly distributed in the matrix. Indeed, assuming that each interstitial atom affects only the nearest six Fe atoms, we calculate that about $24/(0.94(1 - 0.04)) = 26.5$ at. pct Fe atoms can contribute to the second component at a 4 at. pct excess-nitrogen concentration, which is close to the observed 27.5 pct for the intensity of the second component in the MS spectrum for the corresponding sample. The contribution of Fe atoms neighboring with Ti and N atoms inside and on the periphery of the precipitates is insignificant, compared to the uncertainties in the intensity of the second component. Figure 8 demonstrates also that the intensity of the second component is less in the Ti alloy nitrided at 400 °C, 20

hours, and $R_N = -6.8$, pointing to a decrease of Fe atoms with neighboring N atoms. This confirms the decrease of the excess-nitrogen content, in correlation with a decrease of the overall dilation of the matrix (Figure 11). Because, according to observation 2, the size of the Ti-N precipitates does not change significantly, we ascribe the effect to a rearrangement of the atoms in the GP-like cluster. It is hard to say how this rearrangement occurs, *i.e.*, in one step to a stoichiometric TiN precipitate, or by a gradual loss of Fe, and possibly, excess N atoms from the precipitate. If the transition would be gradual, then the fraction of excess nitrogen remaining after reduction at temperatures up to 500 °C could be explained as an N fraction bound to a GP-like cluster. Note that this rearrangement does not occur during the reduction at 300 °C: after the reduction at this temperature, the amount of nitrogen is completely restored after renitriding, in contrast with the processing at 400 °C (Figure 13). Note also that, after 2 hours nitriding at 400 °C, this rearrangement is far from complete. As can be seen in Figures 11 and 13, in this case, the amount of excess N is even slightly larger than after nitriding at 300 °C.

As mentioned before, the excess-nitrogen content is governed by the strain in the matrix, caused by the coherency at interfaces with precipitates. Indeed the data points in Figure 11 are lying much above a linear Vegard-type dependence of the lattice parameter on the excess-nitrogen content, depicted by a solid line with $(\Delta a/\Delta[N]) = 8.0 \times 10^{-4}$ nm/at. pct, as obtained by References 38 and 29 for pure Fe. If the matrix were dilated homogeneously, a larger amount of nitrogen would be dissolved for a particular matrix dilation if the preceding relation is assumed. The reason for this discrepancy is connected with a nonuniformity of the lattice dilation. Whereas, in Figure 11, the lattice constant corresponding to the peak position in the XRD spectrum caused by the strained component is plotted on the vertical scale, and the average value of the excess nitrogen is depicted on the horizontal scale. Note that, in Figures 9 and 10, the peaks have a shoulder at the side of larger angles, *i.e.*, smaller lattice constants. Thus, Figure 11 actually indicates that the excess nitrogen is also distributed inhomogeneously. Evidently, a larger amount of nitrogen is dissolved in the vicinity of the precipitates where the strain is maximal. The same phenomena can be observed for the Cr-containing alloys.

V. CONCLUSIONS

The main conclusions can be summarized as follows.

1. Small (with dimensions of $2.5a_{TiN} \times 2.5a_{TiN} \times 0.5a_{TiN}$) coherent Ti(Fe)N clusters, probably of the GP-zone type, are formed during nitriding at $T = 300$ °C. The GP-like cluster may contain more N atoms than Ti atoms. The presence of these coherent clusters enhances the dilation of the matrix, which leads to an uptake in the Fe matrix of excess N to a concentration as high as 3.5 to 4 at. pct. The clusters grow to larger lateral dimensions during treatments at higher temperatures. In this process, the GP-like clusters loose Fe and N atoms to become stoichiometric TiN precipitates. The precipitates become semicoherent; the lattice becomes less dilated; and the excess nitrogen content decreases.
2. There is no evidence of precipitate formation in the Cr alloy at $T = 300$ °C, while at 400 °C and higher, precipitates form as thin (1 to 2 monolayers) and wide (more than $5a_{CrN}$) platelets, causing a smaller dilation and a much lower excess-nitrogen content. There is no indication that GP-like precipitates are formed in the Cr-containing alloy at any stage.
3. Because of a high concentration of defects in cold-rolled foils, there is no strong tendency for the formation of precipitates at grain boundaries. The precipitates are forming in the bulk of the grains even during nitriding at 500 °C.
4. The strain of the matrix containing Ti-N-(Fe) clusters and precipitates is notably larger than the strain in the matrix containing Cr-N precipitates. The distribution of the matrix strain is not uniform. In the Ti-containing samples, the whole matrix is strained, although not homogeneously. The magnitude of the dilation depends on the temperature of the nitriding or reduction. In contrast, not the magnitude of the strain, but the fraction of the strained matrix does vary significantly with the temperature of nitriding in the Cr-containing alloy, peaking at the lowest temperature of formation of the CrN precipitates.
5. The uptake of nitrogen is the result of the strain in the matrix caused by the presence of the precipitates. Much more nitrogen is taken up in the Ti-containing alloy than in the Cr-containing alloy. Like the strain, the excess-nitrogen concentration is inhomogeneously distributed.

ACKNOWLEDGMENTS

This work was financially supported by the Dutch Technology Foundation (STW), project GWN.4561, and by the Netherlands Institute of Metal Research (NIMR).

APPENDIX
The origin of diffused streaking

In the theory of diffraction from small volumes, platelets are represented in reciprocal space by rods (instead of dots), oriented perpendicular to the plane of the platelet.[25,39] If the incident electron beam is approximately in the plane of thin platelets, then such reciprocal rods produce streaks in the diffraction pattern parallel to the rods. The amplitude of the diffracted electron beam is determined by the structural factor F_g; the parameter, s, which is a deviation of the reciprocal vector from the reciprocal lattice point; and the thickness of the diffracted object h *via*

$$A \sim F_g\,[\sin(\pi hs)/\pi s] \qquad [A1]$$

The s parameter characterizes the length of the streaks in the DP for precipitates of a thickness of several interatomic spacing, and is inversely proportional to the thickness $s \sim 1/h$. For a rectangular box with sizes, h_a, h_b, h_c, we write in a similar way

$$A \sim \sin(\pi h_a s_a)/(\pi s_a)\,\sin(\pi h_b s_b)/(\pi s_b)\,\sin(\pi h_c s_c)/(\pi s_c) \qquad [A2]$$

where s_a, s_b, and s_c are the deviations from the reciprocal lattice points along the directions a^*, b^*, and c^* of the reciprocal lattice. Thus, the width or diffusioness of the streaks can also be considered as a measure of the width of the precipitates, in addition to thickness, determined from the length of the streak. With a width of the streaks of

about 1/10 of $|\mathbf{g}_{200\alpha\mathrm{Fe}}|$ and a length of the streaks of about $\sim|\mathbf{g}_{200\alpha\mathrm{Fe}}|/2$, we arrive at a width of the precipitate of about 1.5 nm and a thickness of ~0.2 to 0.3 nm, *i.e.*, about 1 to 2 monolayers thick by about 10 monolayers wide. Assuming that the extension in the third direction, *i.e.*, parallel to the beam, is equal to the width, we obtain for the precipitates size about $2.5a_{\mathrm{TiN}} \times 2.5a_{\mathrm{TiN}} \times 0.5a_{\mathrm{TiN}}$, or about 30 to 50 Ti-atom sites.

The structural factor F_g in Eq. [A1] is proportional to the atomic scattering amplitude $f(\theta)$:[39]

$$F_g \propto f(\theta) = 2.38 \times 10^{-10} (\lambda/\sin\theta)^2 (Z - f_x) \quad [A3]$$

where θ is the scattering angle, λ is the wavelength, Z is the charge of nuclei, and f_x is the atomic scattering factor for X-rays. From the tables of atomic scattering amplitudes (*i.e.*, Reference 39), one can conclude that the difference between the values for Ti, Cr, and Fe is not large and cannot explain the weaker contrast of streaks in the case of nitrided Ti-containing alloy, as compared with Cr-containing alloy Figures 1 and 2. Evidently, this weakness is due to the fact that the streaks in Ti-containing alloy are wider.

REFERENCES

1. A. Fry: *J. Iron Steel Inst.*, 1932, vol. 125, p. 191.
2. V.A. Phillips and A.U. Seybolt: *Trans. TMS-AIME*, 1968, vol. 24, pp. 2415-22.
3. B. Mortimer, P. Grieveson, and K.H. Jack: *Scand. J. Met.*, 1972, vol. 1, pp. 203-09.
4. D.H. Kirkwood, O.E. Anasoy, and S.R. Keown: *Met. Sci.*, 1974, vol. 8, pp. 49-55.
5. D.H. Jack: *Acta Metall.*, 1976, vol. 24, pp. 137-46.
6. H.H. Podgurski and F.N. Davis: *Acta Metall.*, 1981, vol. 29, pp. 1-9.
7. D.S. Rickerby, A. Henry, and K.H. Jack: *Heat Treatment '81*, The Metal Society, London, 1983, pp. 130-36.
8. D.S. Rickerby, S. Henderson, A. Henry, and K.H. Jack: *Acta Metall.*, 1986, vol. 34, pp. 1687-99.
9. M. Pope, P. Grievenson, and K.H. Jack: *Scand. J. Metall.*, 1973, vol. 2, p. 29.
10. M.M. Yang and A.D. Krawitz: *Metall. Trans. A*, 1984, vol. 15, pp. 1545-54.
11. D.L. Speirs, W. Roberts, P. Grieveson, and K.H. Jack: *Proc. 2nd Int. Conf. on Strength of Metals and Alloys*, Monterey, CA, ASM, Metals Park, OH, 1970, pp. 601-742.
12. J.H. Driver and Papazian: *Acta Metal.*, 1973, vol. 21, pp. 1139-49.
13. K.H. Jack: *Scand. J. Metall.*, 1972, vol. 1, p. 195.
14. A. Krawitz and R. Sinclair: *Phil. Mag.*, 1975, vol. 31, pp. 697-712.
15. D.S. Rickerby, A. Henry, and K.H. Jack: *Acta Metall.*, 1986, vol. 34, pp. 1925-32.
16. D.S. Rickerby and A. Henry: *Acta Metall.*, 1986, vol. 34, pp. 1911-23.
17. M.A.J. Somers, R.M. Lankreijer, and E.J. Mittemeijer: *Phil. Mag. A*, 1989, vol. 59, pp. 353-78.
18. P.M. Hekker, H.C.F. Rozendaal, and E.J. Mittemeijer: *J. Mater. Sci.*, 1985, vol. 20, pp. 718-29.
19. E.H. du Marchie van Voorthuysen, B. Feddes, N.G. Chechenin, D.K. Inia, A.M. Vredenberg, and D.O. Boerma: *Phys. Status Solidi (a)*, 2000, vol. 177, pp. 127-33.
20. E. Lehrer: *Z. Electrochemie*, 1930, vol. 30, pp. 383-92.
21. E.H. du Marchie van Voorthuysen, N.G. Chechenin, and D.O. Boerma: *Metall. Mater. Trans. A*, 2002, vol. 33A, pp. 2593-98.
22. N.G. Chechenin, A. Van Veen, R. Escobar Galindo, H. Schut, A. Chezan, and D.O. Boerma: *Mater. Sci. Forum*, 2001, vols. 363–365, pp. 493-95; *J. Phys.: Condens. Matter*, 2001, vol. 13, pp. 5937-46.
23. N.G. Chechenin, P.M. Bronsveld, A. Chezan, C.B. Craus, D.O. Boerma, J. Th. M. de Hosson, and L. Niesen: *Phys. Status Solidi (a)*, 2000, vol. 177, pp. 117-25.
24. A. Guinier: *X-Ray Diffraction*, W.H. Freeman & Co., San Francisco, 1963, pp. 121-25.
25. G. Thomas: *Transmission Electron Microscopy of Metals*, John Wiley & Sons, New York, NY, 1962, pp. 17-50.
26. S.H. Chen and J.W. Morris: *Metall. Trans. A*, 1977, vol. 8A, pp. 19-26.
27. M.H. Biglari, C.M. Brackman, and E.J. Mittemeijer: *Phil. Mag. A*, 1995, vol. 72, pp. 1281-99.
28. G.P. Huffman and H.H. Podgurski: *Acta Metall.*, 1975, vol. 23, pp. 1367-79.
29. H.A. Wriedt, N.A. Gokcen, and R.H. Nafziger: *Bull. Alloy Phase Diagrams*, 1987, vol. 8, (4), pp. 355-77.
30. H.J. Goldschmidt: *Interstitial Alloys*, Butterworth and Co., London, 1967, pp. 215-53.
31. J.D. Eshelby: *Proc. R. Soc., Ser. A*, 1957, vol. 241, pp. 376-96.
32. J.K. Lee and W.C. Johnson: *Acta Metall.*, 1978, vol. 26, pp. 541-45.
33. Y. Adda and J. Philibert: *La Diffusion Dans Les Solides*, Institute National des Sciences et Techniques Nucléaires, Saclay, 1966, pp. 1167-71.
34. E.J. Mittemeijer, A.B.P. Vogels, and P.J. van der Schaaf: *J. Mater. Sci.*, 1980, vol. 15, pp. 3129-40.
35. J.N. Loquet, R. Sato, L. Barraliier, and A. Charaï: *Microsc. Microanal. Microstr.*, 1997, vol. 8 pp. 335-52.
36. F.R.N. Nabarro: *Proc. R. Soc.*, 1940, vol. A175, pp. 519-38.
37. D.A. Porter and K.E. Easterling: *Phase Transformation in Metals and Alloys*, Chapman & Hall, London, 1992, pp. 192-98.
38. H.A. Wriedt and L. Zwell: *Trans. TMS-AIME*, 1962, vol. 224 (12), pp. 1242-46.
39. P. Hirsh, A. Howie, R.B. Nicholson, D.W. Pashley, and M.J. Whelan: *Electron Microscopy of Thin Crystals*, 2nd ed. R.E. Krieger Publishing Co., Huntington, New York, NY, 1977, pp. 85-107 and 503-05.